Monte Carlo Simulation of Concentrated Diblock Copolymers in a Selective Solvent: Anisotropy of the Diffusion

Moon Bae Ko and Wayne L. Mattice*

Institute of Polymer Science, The University of Akron, Akron, Ohio 44325-3909

Received February 16, 1995; Revised Manuscript Received June 14, 1995[⊗]

ABSTRACT: Monte Carlo simulations were performed with self- and mutually-avoiding symmetric diblock chains on a cubic lattice with periodic boundary conditions. The concentration of diblock copolymer was varied to cover a wide range of volume fraction, 0.45–0.85. The empty lattice sites were treated as a selective solvent, so that the insoluble blocks were seen to aggregate into various morphologies. Spherical, cylindrical, monocontinuous catenoid-lamellar (mesh) and lamellar morphologies were observed as a function of increasing concentration, in that order. The cylindrical morphology changed to monocontinuous catenoid-lamellar morphology by adhesion of nearest-neighbor cylinders, as the concentration of diblock copolymer increases. The concentration at which the transition between morphologies occurs can be identified by analysis of the anisotropy of the translational diffusion coefficient.

Introduction

The variation in morphology of self-assembled diblock copolymer solutions and melts originates from the thermodynamic requirement associated with the incompressibility of polymeric liquids, *i.e.*, the demand of uniform filling of the segments in domain space with the minimum free energy, while keeping the segment density of each domain equal to the segmental density of the respective bulk homopolymers. If the component of the radius of gyration of the A-block parallel to the interface is similar to that of the B-block, interfaces of zero curvature are preferred in order to achieve uniform segmental distribution in domain space with the minimum free energy. The result is lamellar microdomains. However, if the component of the radius of gyration parallel to the interface differs for the A-block and B-block, uniform packing of block chains in domain space with minimum free energy is possible only when the interfaces have a finite curvature. This curvature causes the formation of spherical microdomains, cylindrical microdomains, and so forth. The morphological changes will be observed also by changing the selectivity of the casting solvent for the A-component in solution-cast films or by the addition of the homopolymer of A, simply because the selectivity changes the ratio between the effective radii of gyration of A- and B-block chains.[1–3]

Till recently, most of the observed phenomena for diblock copolymers were understood as follows: As the volume fraction of the minor component (say A) changes from 0 to 0.5, the geometry of the A and B regions varies from spheres of A followed by cylinders of A in a continuous matrix of B to alternating lamellae of A and B. The situation has changed dramatically with the reports of bicontinuous[4,5] and mesh[2,6] microphase structures in solvent-free copolymer melts. These morphologies can be characterized by the two local principal curvatures of the surface. The broadest local classification of surfaces encompasses three geometric classes: hyperbolic (saddle-shaped, negative Gaussian curvature), parabolic (zero Gaussian curvature, *e.g.*, cylinders, planes), and elliptic (positive Gaussian curvature, *e.g.*, spheres). Thus the variation in the morphology of the self-assembly of diblock copolymers can be summarized in Figure 1 as the sequence sphere (elliptic), cylinder (parabolic), many kinds of structures with hyperbolic surfaces, and plane (parabolic).

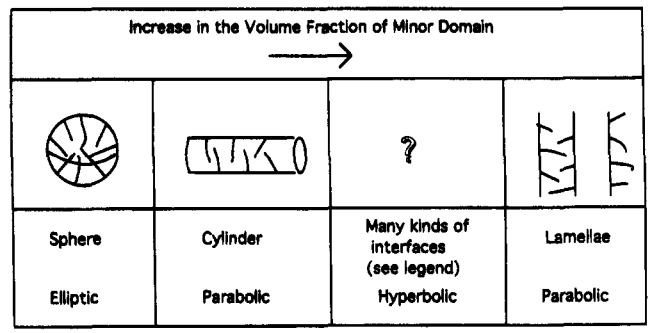

Figure 1. Phase diagram of the morphology of self-assembled diblock copolymers. Structural candidates for the hyperbolic phase include OBDD,[4–6,10] mesh (monocontinuous catenoid-lamellae) and strut (bicontinuous catenoic-lamellar),[1,6] and gyroid.[12]

It is of interest to find new structures in the hyperbolic phase, where the interfaces are periodic saddle-shaped surfaces related to the classical infinite periodic minimal surface of primitive cubic symmetry. The OBDD phase, which was reported at copolymer compositions intermediate between lamellar and cylindrical phases, had not been anticipated theoretically. After its discovery, Anderson and Thomas[7] used the method of Ohta and Kawasaki[8] to estimate the free energy of the OBDD structure but were not successful in predicting its stability relative to cylinders and lamellae. They found, however, that the degree of metastability was minimized in the composition range where the structure was reported. Their work and others[9] suggests that other classes of area-minimizing structures could be candidates for equilibrium microphases in block copolymers. Experimental distinction between different types of structures may be difficult.[10]

After this suggestion, Almdal *et al.*[11] proposed a continuous catenoid-lamellae assembly, in which the lamellae of the minor component are perforated by catenoid-like tubes of the major component. Fredrickson calculated the free energy of this catenoid lamellae and concluded that it should be metastable with respect to both cylinders and lamellae in the strong segregation limit.[6] Hajduk *et al.*[12] reported the identification of a new equilibrium microdomain morphology in an intermediate to weakly segregated diblock copolymer melt.

[⊗] Abstract published in *Advance ACS Abstracts,* August 15, 1995.

0024-9297/95/2228-6871$09.00/0 © 1995 American Chemical Society

Figure 2. Snapshots for self-assembly at $\phi = 0.45$, $\epsilon = 0.5$. The connections between the A-beads are indicated with the short solid lines. The long solid lines outline the periodic cubic cell. The arrow defines the axis for the rotation discussed in the text.

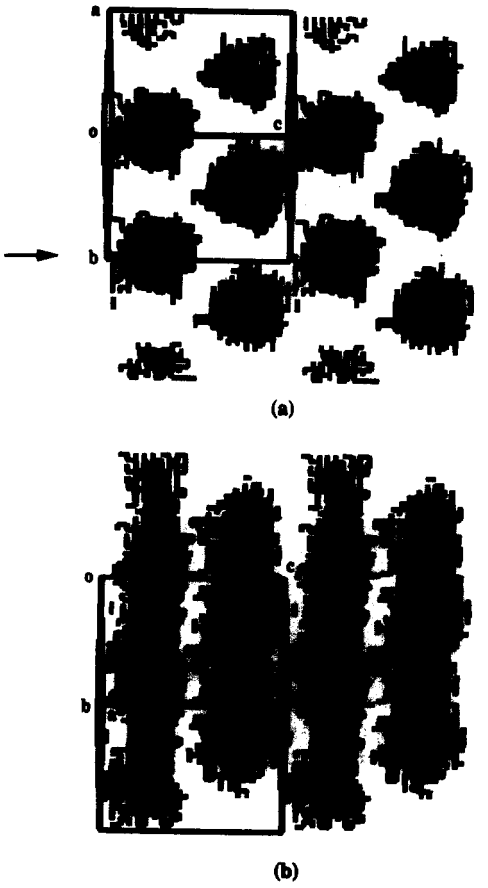

Figure 3. Snapshots for the self-assembly at $\phi = 0.55$, $\epsilon = 0.5$. The views are in the direction (a) of the axis of the cylinder and (b) perpendicular to the axis of the cylinder.

A poly(styrene-*block*-isoprene) transformed from the lamellar morphology to a new morphology at annealing temperatures approximately 50 deg below the order–disorder transition. From computer simulations of model structures and comparison with microscopic results, they proposed models for the new morphology based on the triply periodic G minimal surface (gyroid) discovered by Schoen.[13] Interestingly, Sakurai *et al.*[14] suggested a zippering mechanism by which the cylindrical morphology converts into lamellae when a mixture of poly(styrene-*block*-butadiene-*block*-styrene) triblock copolymers and a polystyrene-selective solvent was dried.

This paper is concerned with the change of morphology with the volume fraction of diblock copolymer and the mechanism by which one type of ordered structure is converted into another, as deduced from the simulation of AB diblock copolymers on a cubic lattice. We focus especially on the mechanism by which cylindrical morphology converts to lamellar and the manner in which this transition affects the anisotropy of the translational diffusion coefficient.

Model and Simulation Technique

Simulations were performed on a cubic lattice with edge length $L = 22$, using periodic boundary conditions. The periodicity of the box affects the spacings of the lamellae that can be observed in the simulations.[15-18] Since determining the anisotropy of the translational diffusion coefficient in the ordered systems requires extensive computation after the systems have equilibrated, we have selected a small periodic box. A periodic box of the size used is small enough to permit spontaneous self-assembly in reasonable simulation time, permits formation of lamellae of $A_{10}B_{10}$ that are not subject to an artificial stress due to the periodicity of the box, and also permits evaluation of the diffusion coefficient in these structures.[19] At the same time, it is large enough to permit formation of the morphologies of interest.

Each chain was modeled as a string of N connected beads. For the simulations reported here, only symmetric chains with $N_A = N_B = 10$ were used. All simulations employ self- and mutually-avoiding chains and a reduced pairwise interaction energy, ϵ, that is applied whenever nonbonded segments of A and B are nearest neighbors. The voids are treated as being energetically equivalent to segments of B. All other pairwise interactions are zero. One Monte Carlo time step is defined here as one trial of reptation and kink-jump bond motion per each segment, on the average.

The simulations were performed as a function of the volume fraction of diblock copolymers, ϕ, covering the range 0.45–0.85 at intervals of 0.05. At each concentration, the system was generated by placing the appropriate number of diblock chains as ordered linear rods on the lattice. The system was equilibrated using the Metropolis rule and $\epsilon = 0$.[20] The resulting random system was used as the starting point for the simulations with $\epsilon > 0$. In each cycle, ϵ was incremented by 0.1 and the system was allowed to equilibrate. The cycles were continued until the system self-assembled into an equilibrium morphology. This method can be equated to the process of annealing, because a step increase in ϵ corresponds to a step decrease in temperature for a real sample. The number of the various contacts in the system may be obtained by inspecting each bead for its neighbors. As the simulation proceeds, contacts with repulsive interactions must decrease to a minimum and those without, increase to a maximum. The numbers of the various contacts were written out at periodic intervals. A plot of the number of contacts against time was used to judge if the system was equilibrated or simulations were to be continued with the same energetics.

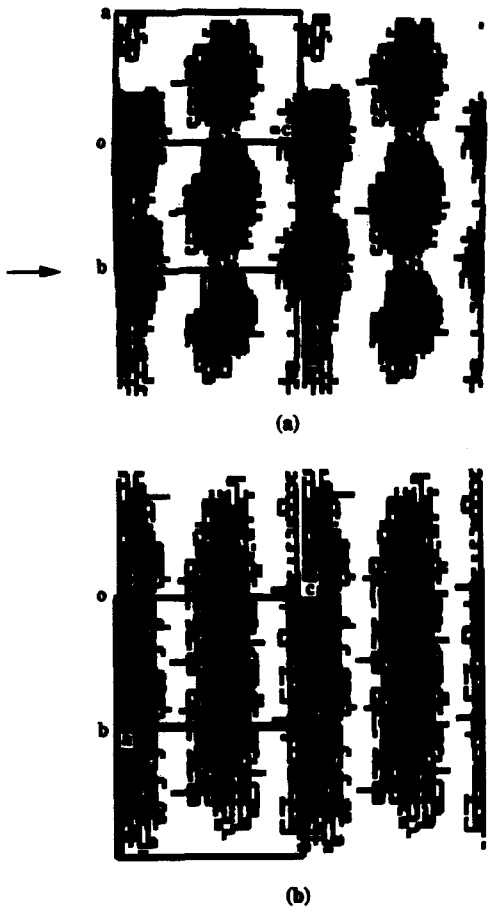

Figure 4. Snapshots for self-assembly at $\phi = 0.70$, $\epsilon = 0.5$. The views are in the direction (a) of the axis of the cylinder and (b) perpendicular to the axis of the cylinder.

Results and Discussion

Visual Identification of Morphologies. Before examining the diffusion coefficients, we describe the static structures that form spontaneously over the range of ϕ covered in the simulations. Snapshots of static replicas can be used to identify the morphologies. Figure 2 is a snapshot of the box and three periodic images of the morphology at $\phi = 0.45$. The orientation of the box with the parent structure distinguishes the viewing angles of the two panels. A plane with three periodic images was rotated to *ca.* 45° about the axis indicated with the arrow in Figure 2a. Figure 2a shows that the domain of the minority component (A-block) is spherical. Figure 2b is the snapshot rotated an additional *ca.* 90° about the axis indicated with the arrow in Figure 2a. The spherical domains are packed on a body-centered cubic lattice in a matrix B even through the domains appear to be hexagonally packed in the two-dimensional projection in this figure.[21] The snapshot (not shown) for the self-assembly at $\phi = 0.50$ shows similar spherical domains. Ordered arrays of spheres have also been observed in simulations of smaller diblock copolymers.[16]

Figure 3 is a snapshot of the box and three periodic images of a self-assembled morphology at $\phi = 0.55$. The minority domains (A-block) in Figure 3a look spherical and are packed in a hexagonal array. Figure 3b is the snapshot rotated an additional *ca.* 90° about the axis indicated with the arrow in Figure 3a. It is seen that the minority domains form cylindrical rods. The spherical domains change into cylindrical ones at ϕ between 0.50 and 0.55 in this simulation. Cylindrical morphologies of dispersed domains were also found at ϕ of 0.60 and 0.65. A similar morphology has been observed with simulations of shorter diblock copolymers.[16]

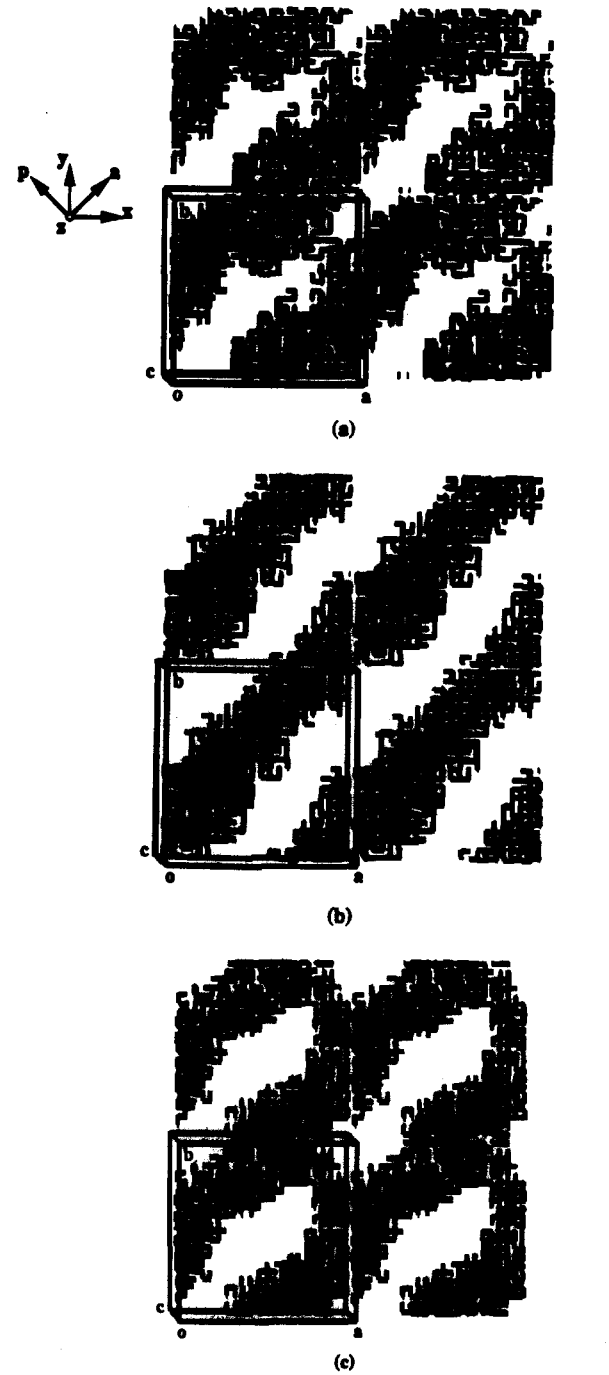

Figure 5. View along the z axis (perpendicular to the a–p plane) at (a) $\phi = 0.70$, $\epsilon = 0.5$, (b) $\phi = 0.65$, $\epsilon = 0.5$, and (c) $\phi = 0.70$, $\epsilon = 0.6$.

Figure 4 is a snapshot of the self-assembled morphology at $\phi = 0.70$. It is cylindrical, but the spherical projections in Figure 4a make a small contact with each other. Parts a and b of Figure 5 are snapshots of a hexagonal array of cylinders, as seen in the direction parallel and perpendicular, respectively, to the cylinder axes. For the purpose of clarity we show only one plane of cylinders. Figure 5a is the snapshot for the middle part of the minority domains in the box. The cylinders, which are arranged in the diagonal direction of the square, adhere to one another at a few positions. In order to compare these adhering cylinders with nonadhering cylinders, the snapshot for $\phi = 0.65$ along the

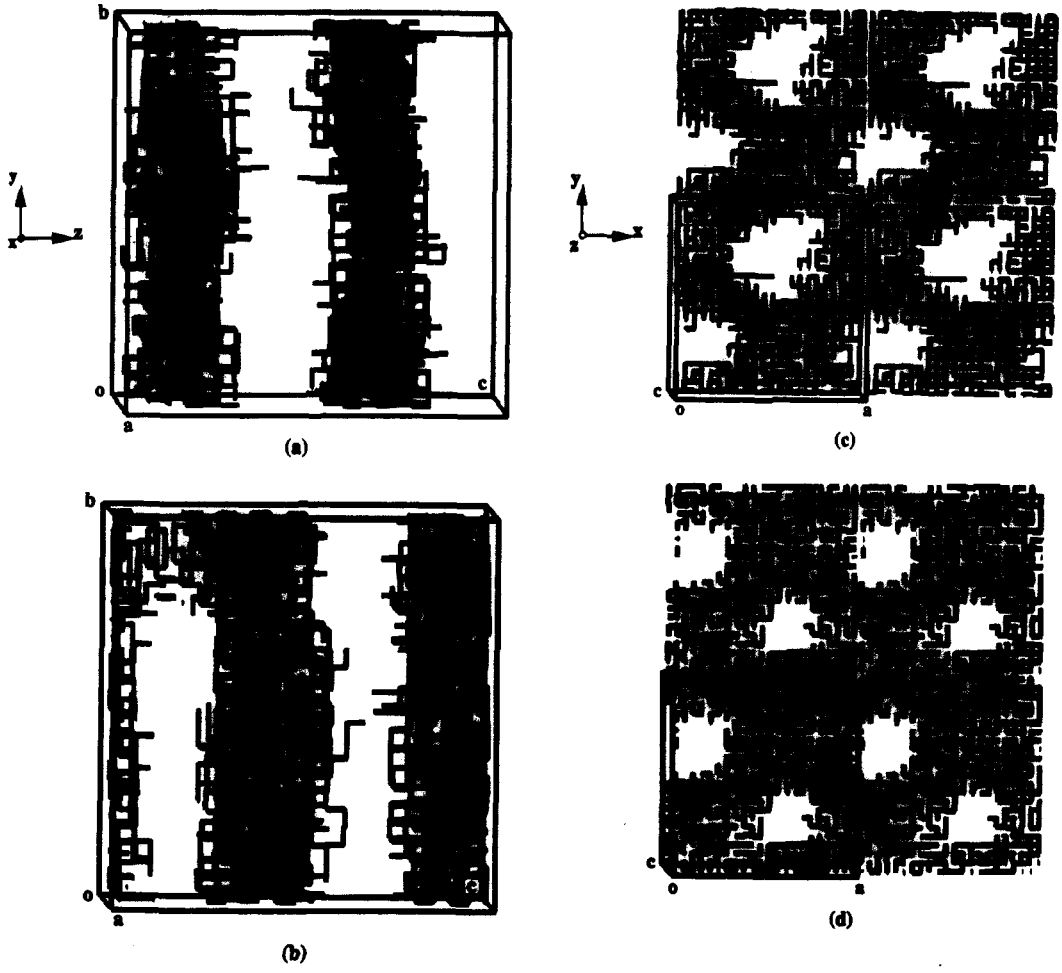

Figure 6. Snapshots at $\phi = 0.75$, $\epsilon = 0.5$, for (a) A-blocks and (b) B-blocks. The A-blocks are also depicted normal to (c) the middle lamella and (d) the outside lamella.

direction normal to the cylinder axis is presented in Figure 5b. The surface on a cylinder for $\phi = 0.65$ looks smoother than that for $\phi = 0.70$ and does not exhibit any adherence between the cylinders.

Sakurai *et al.*[14] proposed a transition scheme from the cylindrical morphology to a lamellar one in which the coalescence of the cylinders may be more reasonable from the viewpoint of the lower energy barrier than a transition scheme that involves the disordering of the system. They studied a mixture of a poly(styrene-*block*-butadiene-*block*-styrene) triblock copolymer and a polystyrene-selective solvent. When the undulating interfaces randomly approach each other and coalesce, channels can be formed between the adjacent cylinders, as can be seen in Figure 5a,c. Undulation is induced by the instability of the interface, which in turn is caused by the change in the interfacial curvature. This undulation might play an important role for the coalescence of the cylinders. Balaji has seen helical structures in simulations near this concentration.[22] Helical structures have a constant mean curvature surface,[23] but such macrostructures have neither been observed experimentally in diblock copolymers, nor predicted by theory.

Parts a and b of Figure 6 are snapshots of the A-blocks and B-blocks at $\phi = 0.75$. The lamellae of the B-blocks are linked to each other with some tie chains, Figure 6b, but the lamellar domains of the A-blocks are not connected, Figure 6a. Parts c and d of Figure 6 are the snapshots taken normal to the lamellar domain ((c) and (d) are the snapshots of the middle lamellae and outside one, respectively) of the A-block, combined with three periodic images taken normal to the lamellar domain. The white space shows where the lamellar planes are perforated with some tie chains of the B-block and solvent selective to the B-block. The two perforations in the lamellae in the parent box produce a tetragonal array with the perforations in the periodic images. These mesh sheets are expected to stack into parallel layers with the tunnel holes of each layer centered over the pores of neighboring layers. This stacking produces mesh morphologies of body-centered tetragonal symmetry. Perforations in the lamellae have also been observed in simulations reported by Larson.[17]

The morphology for $\phi = 0.75$ is very similar to computer-generated parallel stacks of the square mesh structure suggested by Hashimoto *et al.*[2] Theoretical understanding of the stability of this mesh phase is less straightforward. Recent calculations by Fredrickson[6] fail to explain the presence of such a phase in the strong segregation limit of pure diblock copolymers. In his derivation, the free energy was decomposed into contributions from the A "core" region, the B "corona" region, and the interfacial region. The interfacial contribution was considered to be simply the product of the interfacial tension, $\gamma \sim kT\chi b^{-2}$, in which χ and b are the Flory–Huggins interaction parameter and Kuhn statistical segment length, respectively. However, it appears that the contribution for the interfacial free energy from the variation in interfacial curvature was not considered.

Figure 7 depicts the snapshots of the parallel view of

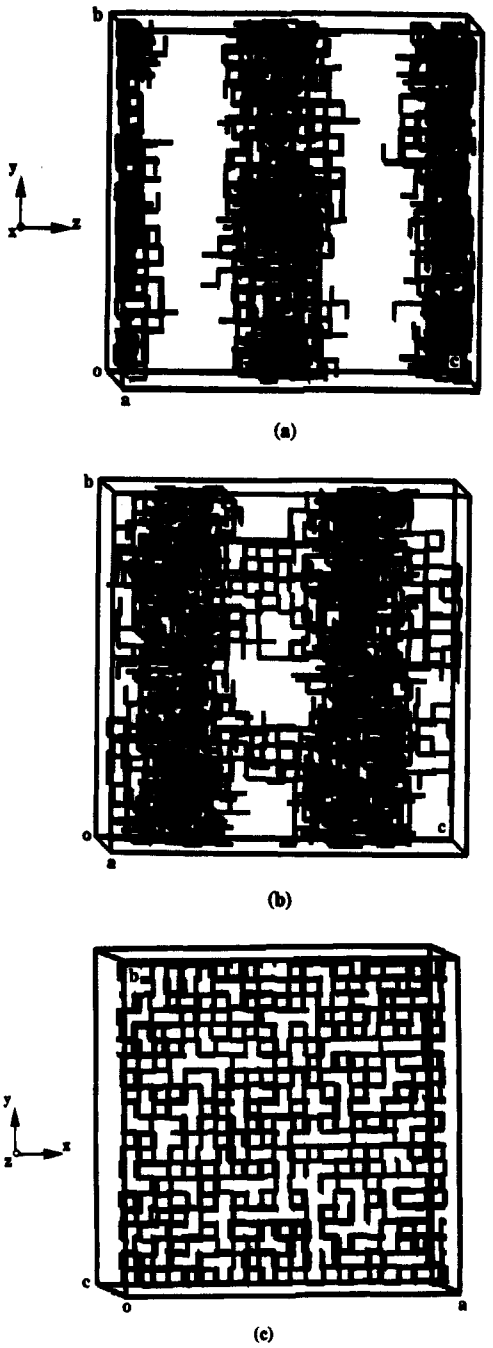

Figure 7. Snapshots at $\phi = 0.80$, $\epsilon = 0.5$, for (a) A-block parallel to the lamellae, (b) B-block parallel to the lamellae, and (c) the unperforated lamella of the A-block, perpendicular to the lamellae.

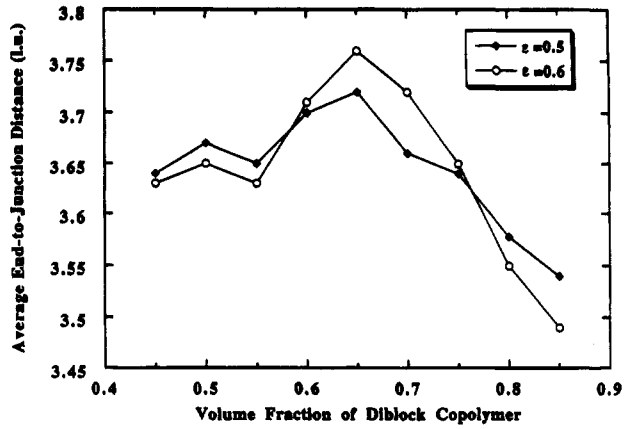

Figure 8. Average end-to-junction distance of the A-block, as a function of ϕ.

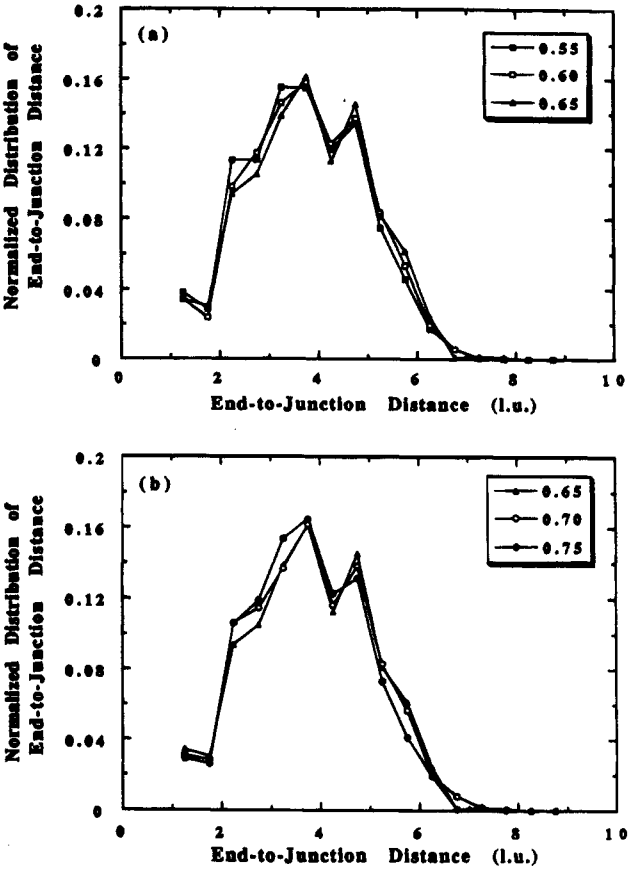

Figure 9. Normalized distribution functions for the end-to-junction distance of the A-block for $\epsilon = 0.5$ and ϕ of (a) 0.55–0.65 and (b) 0.65–0.75.

the (a) A-blocks, (b) B-blocks, and (c) perpendicular view of the A-blocks. Contrary to the perpendicular view of the lamellae for $\phi = 0.75$, there is not perforation in one of the two A-lamellae for $\phi = 0.80$. The transition from the perforated lamellae to the pure lamellae occurs at a concentration of about 0.80 in this simulation.

Numerical Analysis. Figure 8 depicts the average end-to-junction distance, $\langle r \rangle$, for the A-block, which is the minority component, as a function of ϕ. The end-to-junction distance increases as ϕ increases up to 0.65, and then it decreases as ϕ increases further. The overall change is small. Figure 9a depicts the normalized distribution of r for the volume fractions of block copolymers from 0.55 to 0.65. The population at shorter r decreases, and the population at longer r increases, as ϕ increases up to 0.65. This change results from the fact that the A-blocks are more and more stretched due to the excluded volume interaction between the same species of A-block, keeping the morphology in a hexagonal array of cylinders, as ϕ increases. Figure 9b is the normalized distribution of r of A-block for ϕ from 0.65 to 0.75. Contrary to Figure 9a, the population of the longer r shifts to that of shorter r as ϕ increases further. Visually, the transition from cylindrical morphology to perforated lamellae involves the adhering of two adjacent cylinders in the region of ϕ from 0.65 to 0.75. Thus the highly stretched A-blocks at $\phi = 0.65$ tend to shrink to the original random coils after the two cylinders start to adhere to each other.

The mean-square displacements of the A-beads that are located at the junction of the two blocks have been calculated from the trajectories using the following

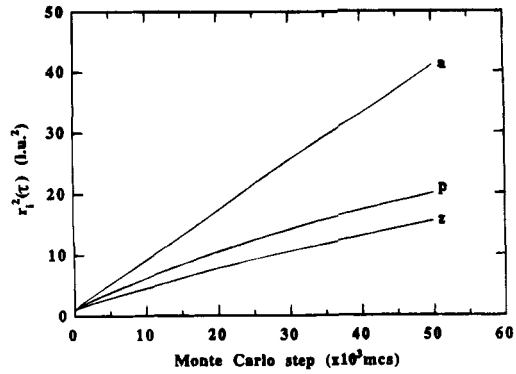

Figure 10. Time evolution for the three components of $r^2(\tau)$ for the A-beads at the junction between the two blocks at $\phi = 0.65$, $\epsilon = 0.5$.

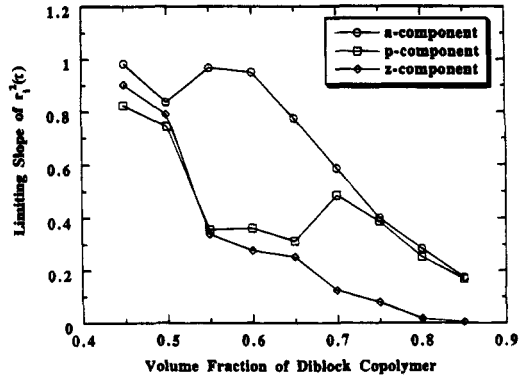

Figure 11. Limiting slope of each component of $r^2(\tau)$ as a function of ϕ, for $\epsilon = 0.5$.

expressions

$$r_i^2(\tau) = \frac{1}{N_c t_{run}} \sum_{j=1}^{N_c} \sum_{t=1}^{t_{run}} [r_{ij}(t+\tau) - r_{ij}(t)]^2 \quad (1)$$

$$r^2(\tau) = \sum_i r_i^2(\tau) \quad (2)$$

where $i = a, p$, and z for displacements along the a, p, and z axes defined in Figure 5. The a axis is along the axis that will be defined by the cylinders when they are present, and the other two axes are normal to a. The p axis is in the plane that will be defined by the lamellae at higher ϕ, and the z axis is normal to this plane (and to the surface of the paper in Figure 5). The number of chains is denoted by N_c, τ is the time interval between observations, expressed in Monte Carlo time steps, and t_{run} is the number of observations. Figure 10 depicts the components of $r^2(\tau)$ for the A-beads at the junction between the two different kinds of blocks for $\phi = 0.65$. This figure shows that the a-component in $r^2(\tau)$ increases more rapidly than the p- and z-components. This anisotropic diffusion results from the fact that the equilibrated morphology itself has an anisotropy. At longer times, $r^2(\tau)$ approaches a behavior that is nearly linear in the number of Monte Carlo time steps. The diffusion coefficient in each direction is proportional to the limiting slope of each component of $r^2(\tau)$.

Figure 11 is the plot of the limiting slope of each component of $r^2(\tau)$, which was obtained from the data in the range of 20 000–50 000 Monte Carlo steps, *vs* ϕ. There are three cases in defining the z-axis for the body-centered cubic lattice morphologies at ϕ values of 0.45 and 0.50. Thus the data for ϕ of 0.45 and 0.50 in Figure 11 are averaged values of limiting slopes for each component of $r^2(\tau)$. The difference between the values of the three components for ϕ of 0.45–0.50 is very small. Upon increasing the concentration from 0.50 to 0.55, the a-component (along the axis of the cylinders) increases abruptly, and the p- and z-components (normal to this axis) decrease. The spherical domains start to adhere to each adjacent spherical domain in the diagonal direction at $\phi = 0.55$, resulting in the formation of cylindrical rods so that the limiting slope of the a-component of $r^2(\tau)$ increases abruptly. Another transition in the limiting slope of the p-component of $r^2(\tau)$ happens in the range of ϕ between 0.65 and 0.70. This component is normal to the axis of the cylinders, and in the plane that will be defined by the lamellae which will be formed at higher ϕ. This transition may be ascribed to the fact that the two adjacent cylinders start to adhere to each other at $\phi = 0.65$. In the lamellar morphology, the diffusion coefficient has two fast (a, p) and one slow (z) components.[19] The slow component is for diffusion normal to the plane of the lamellae.

The change from one morphology to another can be detected from the change in the anisotropy of the translational diffusion coefficient if the measurement is performed with samples with a single coherent grain in the "polycrystalline" macroscopic sample. As ϕ increases, the consecutive changes are from isotropic diffusion, to anisotropic diffusion with one fast and two slow components, to anisotropic diffusion with two fast and one slow components.

Conclusions

In this study the morphological transition from sphere to lamellae was studied by Monte Carlo lattice simulation. Monte Carlo simulations were performed by modeling symmetric diblock chains as self-avoiding walks on a cubic lattice with periodic boundary conditions. Spherical, cylinderical, monocontinuous catenoid-lamellar (mesh), and lamellar morphologies were observed as a function of concentration, in that order. Cylindrical morphology changes to monocontinuous catenoid-lamellar morphology via adherence of two adjacent cylinders, as ϕ increases. This scheme was confirmed by the observation that the population of end-to-junction distance at longer lengths shifts to shorter lengths and that the component of the diffusion coefficient perpendicular to the cylindrical axis increases abruptly after two cylinders start to adhere to each other.

Acknowledgment. We express our thanks to the BF Goodrich Co. and National Science Foundation grant DMR 9220369 for support. M.B.K. thanks the Korea Science and Engineering Foundation for a postdoctoral fellowship and also thanks Dr. Sanjay Misra for helpful discussion and a critical reading of the manuscript.

References and Notes

(1) Tanaka, H.; Hasegawa, H.; Hashimoto, T. *Macromolecules* **1991**, *24*, 240.
(2) Hashimoto, T.; Koizumi, S.; Hasegawa, H.; Izumitani, T.; Hyde, S. T. *Macromolecules* **1992**, *25*, 1433.
(3) Winey, K. I.; Thomas, E. L.; Fetters, L. J. *Macromolecules* **1992**, *25*, 2645.
(4) Thomas, E. L.; Alward, D. B.; Kinning, D. J.; Martin, D. C.; Handlin, D. L.; Fetters, L. J. *Macromolecules* **1986**, *19*, 2197.
(5) Hasegawa, H.; Tanaka, H.; Yamasaki, K.; Hashimoto, T. *Macromolecules* **1987**, *20*, 1651.
(6) Fredrickson, G. H. *Macromolecules* **1991**, *24*, 3456.
(7) Anderson, D. M.; Thomas, E. L. *Macromolecules* **1988**, *21*, 3221.

(8) Ohta, T.; Kawasaki, K. *Macromolecules* **1986**, *19*, 2621.
(9) Förster, S.; Khandpur, A. K.; Zhao, J.; Bates, F. S.; Hamley, I. W.; Ryan, A. J.; Bras, W. *Macromolecules* **1994**, *27*, 6922.
(10) Hajduk, D. A.; Harper, P. E.; Gruner, S. M.; Honeker, C. C.; Thomas, E. L.; Fetters, L. J. *Macromolecules* **1995**, *28*, 2570.
(11) Almdal, K.; Koppi, K. A.; Bates, F. S.; Mortensen, K. *Macromolecules* **1992**, *25*, 1743.
(12) Hajduk, D. A.; Harper, P. E.; Gruner, S. M.; Honeker, C. C.; Kim, G.; Thomas, E. L.; Fetters, L. J. *Macromolecules* **1994**, *27*, 4063.
(13) Schoen, A. H. NASA Technical Report No. 05541, 1970.
(14) Sakurai, S.; Momii, T.; Taie, K.; Shibayama, M.; Nomura, S.; Hashimoto, T. *Macromolecules* **1993**, *26*, 485.
(15) Balaji, R.; Wang, Y.; Foster, M. D.; Mattice, W. L. *Comput. Polym. Sci.* **1993**, *3*, 15.
(16) Larson, R. G. *Chem. Eng. Sci.* **1994**, *49*, 2833.
(17) Larson, R. G. *Mol. Simul.* **1994**, *13*, 321.
(18) Larson, R. G. *Macromolecules* **1994**, *27*, 4198.
(19) Haliloğlu, T.; Balaji, R.; Mattice, W. L. *Macromolecules* **1994**, *27*, 1473.
(20) Metropolis, N.; Rosenbluth, A. N.; Rosenbluth, M. M.; Teller, A. H.; Teller, E. J. *J. Chem. Phys.* **1953**, *21*, 1087.
(21) Bates, F. S.; Fredrickson, G. H. *Annu. Rev. Phys. Chem.* **1990**, *41*, 525.
(22) Balaji, R. Ph.D. Dissertation, The University of Akron, 1994.
(23) Anderson, D. M.; Davis, H. T.; Nitsche, J. C. C.; Scriven, L. E. *Adv. Chem. Phys.* **1990**, *77*, 337.

MA950202T